Attenuation of Transverse Ultrasound in Copper*

ROGER C. ALIG AND SERGIO RODRIGUEZ
Department of Physics, Purdue University, Lafayette, Indiana
(Received 12 December 1966)

We investigate the propagation of shear acoustic waves traveling parallel to a magnetic field along a symmetry direction in a metal crystal. We obtain the propagation constant of ultrasound for the ⟨100⟩ and ⟨111⟩ directions in a single copper crystal using an analytic representation of the conduction-band structure obtained from existing theoretical calculations of the energy eigenvalues of the conduction band. Various characteristic parameters of copper were obtained together with curves showing the attenuation and the rotation of the plane of polarization of shear acoustic waves.

I. INTRODUCTION

THE work of Kjeldaas[1] on the theory of the attenuation of transverse sound waves propagating parallel to an external magnetic field in a pure metal crystal inaugurated a considerable amount of theoretical[2,3] and experimental[4–8] studies. The equation of motion of the lattice in the presence of a shear wave has been considered in connection with the study of the helicon-phonon interaction in metals.[9,10] These authors assume a metal consisting of a free-electron gas embedded in an isotropic background of positively charged ions which are able to sustain both longitudinal and shear acoustic waves. The results of experimental work on potassium[6] using the Kjeldaas geometrical arrangement appear to agree with the free-electron model; however, as one would expect, the results of similar work on copper,[7] tin[8,9] and aluminum[10] do not agree with the free-electron model.

Taking the velocity of sound s in a typical metal to be of the order 10^5 cm/sec, the phonon wavelength will be approximately 10^{-3} cm for ultrasonic waves of frequency 100 Mc/sec. Since this wavelength is much larger than the lattice spacing, we may describe the sound wave by the displacement and velocity fields $\xi(\mathbf{r},t)$ and $\mathbf{u}(\mathbf{r},t) = \partial\xi(\mathbf{r},t)/\partial t$. When an external magnetic field of several thousand gauss is placed parallel to the wave vector $\mathbf{q}$ of the sound wave, the cyclotron frequency of the electrons greatly exceeds the frequency ω of the sound wave; thus, we may consider the sound wave fixed in space. Assuming the mean free path of the electrons to be larger than the wavelength λ of the sound wave, they will gain energy from the sound wave via interaction with the resulting self-consistent electric field. The condition for this to occur for electrons having an average velocity $\bar{v}$ in the direction of the field is

$$\bar{v}T=\lambda, \tag{1}$$

where T is the electronic cyclotron period. Writing the cyclotron frequency of the electron $\omega_c=2\pi/T$ and $q=2\pi/\lambda$, Eq. (1) becomes

$$\omega_c=q\bar{v}. \tag{2}$$

Since the detailed electronic model has little effect on the velocity of shear acoustic waves,[11] we can write $q=\omega/s$, ω being the angular frequency of the sound wave. With this and the definition $\omega_c=eB_0/m_c c$, where m_c is the cyclotron effective mass of these electrons, Eq. (2) can be written in the form

$$B_0=(c\omega/se)m_c\bar{v}. \tag{3}$$

This result implies that the ultrasonic attenuation of shear waves in metals as a function of applied magnetic field shows an absorption edge, which we shall refer to as the Kjeldaas edge, at the magnetic field for which the right side of Eq. (3) is a maximum.

We consider the propagation of a shear elastic wave along a symmetry direction of a metal crystal parallel to an external dc magnetic field. Further, we require that the shear modes be degenerate, i.e., the velocity of sound is independent of the plane of polarization. For example, this occurs in a cubic crystal for propagation along a ⟨100⟩ or ⟨111⟩ direction. In Sec. II we consider the equation of motion of the lattice under these conditions. In Secs. III and IV we apply these results to the calculation of the attenuation of sound in copper metal as a function of magnetic-field strength.

II. THEORY

Taking the force on an ion arising from the short-range ion-core interactions as $Ms^2\nabla^2\xi$, where M is the mass of the ion whose charge will be assumed to be ze, we can write the equation of motion for the displace-

* Supported in part by the Advanced Research Projects Agency and by the National Aeronautics and Space Administration.
[1] T. Kjeldaas, Jr., Phys. Rev. **113**, 1473 (1959).
[2] M. H. Cohen, M. J. Harrison, and W. A. Harrison, Phys. Rev. **117**, 937 (1960).
[3] R. C. Alig, J. J. Quinn, and S. Rodriguez, Phys. Rev. **148**, 632 (1966); Phys. Rev. Letters **14**, 981 (1965).
[4] R. L. Thomas and H. V. Bohm, Phys. Rev. Letters **16**, 587 (1966).
[5] J. D. Gavenda and J. R. Boyd, Phys. Rev. Letters **15**, 364 (1965), and J. R. Boyd, Ph.D. thesis, University of Texas, 1965 (unpublished).
[6] A. R. Mackintosh, Phys. Rev. **131**, 2420 (1963).
[7] B. I. Miller, Bull. Am. Phys. Soc. **10**, 371 (1965).
[8] B. K. Jones, Phil. Mag. **9**, 217 (1964).
[9] D. N. Langenberg and J. Bok, Phys. Rev. Letters **11**, 549 (1963).
[10] J. J. Quinn and S. Rodriguez, Phys. Rev. **133**, A1589 (1964).
[11] S. Rodriguez, Phys. Rev. **130**, 1778 (1963).

ment field of the lattice as

$$\frac{\partial^2}{\partial t^2}\xi = s^2\nabla^2\xi + (\mathbf{F}_e/M), \tag{4}$$

where $\mathbf{F}_e$ represents all other forces exerted on the lattice. These forces include the long-range Coulomb forces of the other ions, as screened by the conduction electrons, the effect of the external magnetic field on the ion and an average collision force resulting from electron-ion interactions. The first two forces may be described in terms of a self-consistent electromagnetic field acting on the electrons and on the positive ions, together with any external fields that may be present. This contribution to $\mathbf{F}_e$ is $ze\mathbf{E}+(ze/c)\mathbf{u}\times\mathbf{B}$, where $\mathbf{E}$ is the self-consistent electric field and $\mathbf{B}$ is the sum of the self-consistent magnetic field and the external dc magnetic field $\mathbf{B}_0$. We can set $\mathbf{B}=\mathbf{B}_0$ since the external field will be much larger than any self-consistent magnetic fields which may arise from the presence of the wave. The average collision force results from the momentum $m(\mathbf{v}-\mathbf{u})$ being transferred to the lattice when an electron of mass m and velocity $\mathbf{v}$ collides with the lattice. Here we have assumed that the electron scattering is isotropic, i.e., all directions of scattering are equally probable, in the frame of reference in which the lattice is locally at rest. If we introduce an average electron-lattice collision time $\tau=\langle 1/\tau(\mathbf{k})\rangle^{-1}$ where the average is taken over all the electrons, i.e., averaged over the Fermi surface, the force $\mathbf{F}_e$ can be written

$$\mathbf{F}_e = ze\mathbf{E}+(ze/c)(\mathbf{u}\times\mathbf{B}_0)+(zm/\tau)(\langle\mathbf{v}\rangle-\mathbf{u}), \tag{5}$$

where $\langle\mathbf{v}\rangle$ is the average electron velocity. The quantity $\langle\mathbf{v}\rangle$ may be related to the electron current density by the equation

$$\mathbf{j}^{(1)} = -n_0e\langle\mathbf{v}\rangle, \tag{6}$$

where n_0 is the number of conduction electrons per unit volume.

Let us assume the space-time dependence of the sound wave is given by $\exp(i\omega t-i\mathbf{q}\cdot\mathbf{r})$, where ω and $\mathbf{q}$ are the angular frequency and wave vector of the sound wave. Within the linear approximation all other quantities dependent on the sound field show the same space-time variation. For convenience, we describe the transverse wave by the circularly polarized parameters $\xi_\pm=\xi_x\pm i\xi_y$ where we have taken a Cartesian coordinate system with the z axis parallel to $\mathbf{B}_0$. Using similarly defined quantities we obtain from Eqs. (4)–(6)

$$\left(\omega^2-s^2q^2\pm\Omega_c\omega-\frac{i\omega zm}{M\tau}\right)\xi_\pm+\left(\frac{ze}{M}\right)E_\pm - \left(\frac{zm}{n_0Me\tau}\right)j_\pm^{(1)}=0, \tag{7}$$

where $\Omega_c=(zeB_0/Mc)$ is the cyclotron resonance frequency of a free ion in the magnetic field B_0. There is, of course, a longitudinal mode resulting from the component E_z of the self-consistent field. However, we take this component to be small and, hence, the interaction of the transverse modes and this longitudinal mode is negligible.

There may also be a force on the lattice from the conduction electrons due to the presence of a deformation potential Φ. Thus, we should add to $\mathbf{F}_e$ the term $-en_0\nabla\Phi$ to include this force. However, Φ is dependent upon the presence of the disturbance, and, hence, must have the same space-time dependence. Therefore, $\nabla\Phi$ can have a nonzero component only in the z direction, i.e., only for the longitudinal mode. Again the effect of the interaction of this longitudinal mode with the transverse modes is negligible.

We now need equations relating $E_\pm$ and $j_\pm^{(1)}$ to $\xi_\pm$. One such relation comes from Maxwell's equation connecting the total current density

$$\mathbf{j}=\mathbf{j}^{(1)}+n_0e\mathbf{u} \tag{8}$$

to the self-consistent electric field $\mathbf{E}$, i.e., $c\nabla\times\mathbf{E}=-(\partial\mathbf{B}/\partial t)$ and $c\nabla\times\mathbf{B}=4\pi\mathbf{j}$. We have neglected the electric displacement in these equations since $\omega\ll cq$. Noting that $\nabla\cdot\mathbf{E}=0$ because we have taken $\mathbf{E}$ to have only transverse components, we have

$$c^2q^2E_\pm=-4\pi i\omega j_\pm. \tag{9}$$

The second such relation is the so-called constitutive equation relating $\mathbf{j}^{(1)}$ to $\mathbf{E}$. The electron current density has a component from the self-consistent field $\mathbf{E}$ and a component from the fact the scattered electrons retain a drift velocity $\mathbf{u}$.[12] There is also a component from the diffusion current resulting from variations in the local electron density. However, the local electron density is constant in the approximation that $E_z=0$, and, hence, we may ignore this term. This constitutive equation, obtained by the standard arguments of transport theory discussed in Refs. 11 and 13, is

$$\mathbf{j}^{(1)}=\boldsymbol{\sigma}\cdot(\mathbf{E}-m\mathbf{u}/e\tau), \tag{10}$$

where $\boldsymbol{\sigma}$ is the magnetoconductivity tensor. Equation (10) may be written in circularly polarized notation as

$$j_\pm^{(1)}=\sigma_\pm[E_\pm-(mi\omega/e\tau)\xi_\pm], \tag{11}$$

where $\sigma_\pm=\sigma_{xx}\mp i\sigma_{xy}$. We have used here the relations $\sigma_{xx}=\sigma_{yy}$ and $\sigma_{yx}=-\sigma_{xy}$ which follow from symmetry considerations of the crystalline model.

From Eqs. (9) and (11) we obtain

$$j_\pm^{(1)}+n_0ei\omega\xi_\pm=(ic^2q^2/4\pi\omega)E_\pm\equiv i\beta\sigma_0E_\pm. \tag{12}$$

The last equality defines the parameter β. $\sigma_0=n_0e^2\tau/m$ is a constant which has the dimensions of a conductivity, but should not be identified with the dc electrical con-

[12] T. Holstein, Phys. Rev. **113**, 479 (1959).

[13] A. W. Overhauser and S. Rodriguez, Phys. Rev. **141**, 431 (1966).

ductivity of the crystal. Substitution of Eq. (11) in Eq. (12) gives

$$E_{\pm}=\frac{mi\omega}{e\tau}\frac{(G_{\pm}-1)}{(G_{\pm}-i\beta)}\xi_{\pm}, \tag{13}$$

with $\sigma_{\pm}=\sigma_0 G_{\pm}$. Substitution of Eq. (13) in Eq. (11) gives

$$j_{\pm}^{(1)}=-\sigma_0 G_{\pm}\frac{mi\omega}{e\tau}\frac{(1-i\beta)}{(G_{\pm}-i\beta)}\xi_{\pm}. \tag{14}$$

With Eqs. (13) and (14), Eq. (7) becomes

$$\left[\omega^2-s^2q^2\pm\Omega_c+\frac{zim\omega}{M\tau}\frac{(1-i\beta)(G_{\pm}-1)}{(G_{\pm}-i\beta)}\right]\xi_{\pm}=0. \tag{15}$$

An equation of the same form as Eq. (15) was derived by Quinn and Rodriguez,[5] who assumed that the metal consisted of an electron gas imbedded in an isotropic background of positively charged ions, and, hence, the longitudinal component of the self-consistent electric field arising in the presence of a transverse acoustic wave was identically zero. We have assumed the existence of a discrete lattice, and neglected the interaction of the longitudinal mode with the transverse modes. As mentioned by Quinn and Rodriguez, solutions of Eq. (15) may be identified with right- and left-circularly polarized acoustic waves and with a left-circularly polarized electromagnetic wave called a helicon.

The magnetoconductivity tensor $\boldsymbol{\sigma}$ is discussed in Ref. 13 where the result

$$\boldsymbol{\sigma}=\frac{2e^3B_0}{(2\pi)^3\hbar^2 c}\int d\epsilon\left(-\frac{df_0}{d\epsilon}\right)\int dk_z\, T(\epsilon,k_z)$$

$$\times\sum_{n=-\infty}^{\infty}\mathbf{V}_n\mathbf{V}_n^*[1/\tau+i(\omega-n\omega_c-\mathbf{q}\cdot\mathbf{v}_s)]^{-1} \tag{16}$$

is obtained, with

$$\mathbf{V}_n(\epsilon,k_z)=\frac{1}{T}\int_0^T du\,\mathbf{v}(u)\exp i[\mathbf{q}\cdot\mathbf{R}_p(u)-n\omega_c u]. \tag{17}$$

The period of motion $T(\epsilon,k_z)$ in $\mathbf{k}$ space of an electron having energy ϵ and a component of its wave vector equal to k_z in the z direction is related to the cyclotron frequency ω_c by

$$\omega_c=\frac{2\pi}{T(\epsilon,k_z)}=\frac{eB_0}{cm_c(\epsilon,k_z)}, \tag{18}$$

where m_c is the cyclotron effective mass of the electron. The function $\mathbf{R}(u)$ which gives the position in real space of an electron of energy ϵ and component k_z of the wave vector at the time u can always be separated into two terms $\mathbf{R}_s(u)$ and $\mathbf{R}_p(u)$ so that $\mathbf{R}=\mathbf{R}_s+\mathbf{R}_p$. Here $\mathbf{R}_p$ is a periodic function of $\mathbf{k}$, while $\mathbf{R}_s=\mathbf{v}_s(\epsilon,k_z)u$ increases linearly with the time u. The function $\mathbf{v}(\epsilon,k_z,u)$ is the velocity of an electron on the orbit defined by ϵ and k_z at the time u, and $\mathbf{v}_s(\epsilon,k_z)$ is the average of this velocity. $f_0=f_0(\epsilon(\mathbf{k}))$ is the electronic distribution in thermal equilibrium, and integration of $-(df_0/d\epsilon)$ over ϵ indicates, of course, that the integral over k_z in Eq. (16) is to be evaluated at the Fermi energy ϵ_F. In circularly polarized notation Eq. (16) becomes

$$\sigma_{\pm}=\frac{e^3B_0}{(2\pi)^3\hbar^2 c}\sum_{n=-\infty}^{\infty}\int dk_z\, T(\epsilon_F,k_z)(V_{n\pm}+V_{n\mp})V_{n\pm}^*$$

$$\times[1/\tau+i(\omega-n\omega_c-\mathbf{q}\cdot\mathbf{v}_s)]^{-1}. \tag{19}$$

If the direction of $\mathbf{B}_0$ is a p-fold axis of rotational symmetry in the crystal, then that direction will be a p-fold symmetry axis for $\epsilon(\mathbf{k})$ in $\mathbf{k}$ space. For example, in a cubic crystal, $p=4$ and 3 for the $\langle 100\rangle$ and $\langle 111\rangle$ directions, respectively. The directions which we consider in a cubic crystal are also such that there exists a plane of mirror symmetry which contains the symmetry direction. If we consider a plane perpendicular to the symmetry direction, it will intersect the mirror symmetry plane in a line which we use as the origin of an angular coordinate φ, i.e., a point in $\mathbf{k}$ space may be designated by the cylindrical coordinates (ρ,φ,k_z) and for a given k_z and ρ

$$\epsilon(\varphi)=\epsilon(-\varphi). \tag{20}$$

Since $\epsilon(\mathbf{k})$ exhibits p-fold rotational symmetry about the direction under consideration, we expand it in a Fourier series as

$$\epsilon(\mathbf{k})=\sum_{l=-\infty}^{\infty}\epsilon_l(\rho,k_z)e^{ipl\varphi}. \tag{21}$$

Using Eq. (20) and the fact that $\epsilon(\mathbf{k})$ is real, we obtain the condition

$$\epsilon_l(\rho,k_z)=\epsilon_{-l}(\rho,k_z), \tag{22}$$

where each $\epsilon_l(\rho,k_z)$ is real.

The transverse components of the electron velocity can be written

$$\hbar v_{\pm}=\left(\frac{\partial\epsilon}{\partial k_x}\pm i\frac{\partial\epsilon}{\partial k_y}\right)=e^{\pm i\varphi}\left(\frac{\partial\epsilon}{\partial\rho}\pm\frac{i}{\rho}\frac{\partial\epsilon}{\partial\varphi}\right). \tag{23}$$

Substitution of Eq. (21) in this expression gives

$$v^{\pm}=\sum_{l=-\infty}^{\infty}w_l{}^{\pm}e^{i(pl\pm1)\varphi}, \tag{24}$$

where

$$w_l{}^{\pm}=w_{-l}{}^{\mp}=\frac{1}{\hbar}\left(\frac{\partial\epsilon_l}{\partial\rho}\mp\frac{pl}{\rho}\epsilon_l\right).$$

Equation (21) also gives the z component of the electron

velocity

$$v_z=\frac{1}{\hbar}\frac{\partial\epsilon}{\partial k_z}=\bar{v}+\sum_{l=1}^{\infty}v_l\cos pl\varphi\,, \tag{25}$$

where $\hbar\bar{v}=\partial\epsilon_0/\partial k_z$ and $\hbar v_l=2(\partial\epsilon_l/\partial k_z)$.

In order to obtain the time dependence of φ we use the relation $\omega_c T(\epsilon,k_z)=2\pi$ to write

$$d\varphi/du=\omega_c+f(\omega_c u)\,,$$

where $f(\omega_c u)$ is a periodic function of the time parameter u with period $2\pi/p\omega_c$. Integrating and neglecting the periodic variation of φ with u, we find

$$\varphi=\omega_c u. \tag{26}$$

The z component of $\mathbf{R}_p(u)$ is given by the periodic part of $\int v_z du$, or

$$R_{pz}=\sum_{l=1}^{\infty}\frac{v_l}{lp\omega_c}\sin pl\omega_c u. \tag{27}$$

Defining $X_l=qv_l/lp\omega_c$ and substituting Eqs. (27) and (24) in Eq. (17) we obtain

$$V_{n\pm}=\frac{1}{T}\int_0^T du\Big(\sum_{l=-\infty}^{\infty}w_l{}^{\pm}e^{ipl\omega_c u}\Big)\times\exp i\Big[\sum_{l=1}^{\infty}X_l\sin pl\omega_c u-n\omega_c u\pm\omega_c u\Big]. \tag{28}$$

Using the expansion[14]

$$\exp(iX\sin\theta)=\sum_{l=-\infty}^{\infty}J_l(X)e^{il\theta}, \tag{29}$$

where $J_l(X)$ is a Bessel function of order l, we write Eq. (28) as

$$V_{n\pm}=\frac{1}{T}\int_0^T du\,\exp[i(\pm1-n)\omega_c u]\times\Big[\sum_{l=-\infty}^{\infty}w_l{}^{\pm}\exp(ipl\omega_c u)\Big]\times\prod_{j=1}^{\infty}\Big[\sum_{l_j=-\infty}^{\infty}J_{l_j}(X_j)\exp(ijpl_j\omega_c u)\Big]. \tag{30}$$

Interchanging product and summation and integrating we have

$$V_{n\pm}=\sum_{l=-\infty}^{\infty}\sum_{l_1,l_2\cdots l_n\cdots}\prod_{j=1}^{\infty}J_{l_j}(X_j)w_l{}^{\pm}\times\delta\Big(n,pl\pm1+\sum_{k=1}^{\infty}kpl_k\Big), \tag{31}$$

where $\delta(i,j)$ is defined to be one if $i=j$ and zero otherwise. Fixing l and adjusting the summation index l_1 we obtain

$$V_{n\pm}=\sum_{l=-\infty}^{\infty}\sum_{l_1,l_2\cdots l_n\cdots}\prod_{j=2}^{\infty}J_{l_j}(X_j)w_l{}^{\pm}J_{l_1-l}(X_1)\times\delta\Big(n,\pm1+\sum_{k=1}^{\infty}kpl_k\Big).$$

Therefore

$$V_{n\pm}V_{n\pm}{}^{*}=\sum_{l_1=-\infty}^{\infty}\sum_{l_2l_2'l_3l_3'\cdots l_nl_n'\cdots}\prod_{j=2}^{\infty}J_{l_j}(X_j)J_{l_j'}(X_j)\times\Big[\sum_{l=-\infty}^{\infty}w_l{}^{\pm}J_{l_1-l}(X_1)\Big]\Big[\sum_{l'=-\infty}^{\infty}w_{l'}{}^{\pm}J_m(X_1)\Big]\times\delta\Big(n,\pm1+\sum_{k=1}^{\infty}kpl_k\Big), \tag{32}$$

where

$$m=l_1-l'+\sum_{k=2}^{\infty}k(l_k-l_k').$$

For $p=3$, 4, or 6, $V_{n\pm}V_{n\pm}{}^{*}=0$. Thus, putting Eq. (32) in Eq. (19) we have

$$\sigma_{\pm}=\frac{e^3B_0}{(2\pi)^3\hbar^2c}\sum_{l_1=-\infty}^{\infty}\sum_{l_2l_2'l_3l_3'\cdots l_nl_n'\cdots}\prod_{j=2}^{\infty}\int dk_z T(\epsilon_F,k_z)\times J_{l_j}(X_j)J_{l_j'}(X_j)\Big[\sum_{l=-\infty}^{\infty}w_l{}^{\pm}J_{l_1-l}(X_1)\Big]\times\Big[\sum_{l'=-\infty}^{\infty}w_{l'}{}^{\pm}J_m(X_1)\Big]\times\Big[\frac{1}{\tau}+i\Big(\omega-\omega_c\Big(\pm1+\sum_{k=1}^{\infty}kpl_k\Big)-q\bar{v}\Big)\Big]^{-1}, \tag{33}$$

where we have substituted $q\bar{v}$ for $\mathbf{q}\cdot\mathbf{v}_s$.

III. APPROXIMATE ANALYTIC REPRESENTATION FOR THE BAND STRUCTURE OF COPPER

The electronic band structure of copper deviates from the free-electron model because of the strong overlap of the s and d energy bands. Thus, an analytic function of $\mathbf{k}$ to represent the conduction-band structure cannot easily be found, although such a description is necessary to obtain the velocity components given by the gradient of $\epsilon(\mathbf{k})$. Recent theoretical calculations of the energy-band structure of copper have been made by Segall,[15] who used the Green's-function method, and by Burdick,[16] who used augmented plane waves to obtain numerically the electronic energy eigenvalues for selected values of the electron wave vector $\mathbf{k}$. Both of these au-

[14] H. B. Dwight, *Tables of Integrals and Other Mathematical Data* (The Macmillan Company, New York, 1961), 4th ed., p. 198.

[15] B. Segall, Phys. Rev. **125**, 109 (1962).

[16] G. A. Burdick, Phys. Rev. **129**, 138 (1963).

thors used the potential derived for copper by Chodorow[17] and their results are in close agreement with one another. Roaf[18] used the experimental frequencies of the de Haas–van Alphen oscillations for various directions of the magnetic field obtained by Shoenberg[19] to fit an analytical expression for the Fermi surface. From this expression he obtained the radius vectors of the Fermi surface for a number of angles. His results are in reasonable agreement with the Fermi surfaces obtained by Burdick and Segall.

We propose to fit an analytical expression for $\epsilon(\mathbf{k})$ to the numerical calculations of these authors. Our results involve the use of Burdick's data only, although we obtained similar results when Roaf's data was incorporated with Burdick's. The first Brillouin zone for the face-centered cubic (fcc) lattice, which is the lattice configuration of copper, was partitioned into 2048 cubical volume elements by Burdick. The energy eigenvalues were then computed for the value of $\mathbf{k}$ lying at the center of each volume element. By reason of the symmetry of the fcc lattice it is necessary to consider only those $\mathbf{k}$ values lying within a one-forty-eighth part of the volume of the Brillouin zone, the energy eigenvalues of all other $\mathbf{k}$ values considered in the first Brillouin zone being equal to those of one of the $\mathbf{k}$ values in this smaller volume. There are 89 $\mathbf{k}$ values in this smaller volume, each of which may then be weighted for the number of $\mathbf{k}$ values in the total Brillouin zone which are equivalent to it by symmetry. The weighting factor for each $\mathbf{k}$ value is given in Table II of Burdick's article,[16] and the energy eigenvalue of the conduction band is given in Table III of the same article. The frame of reference used by Burdick was one in which the Cartesian axes of $\mathbf{k}$ space lie along the $\langle 100\rangle$ directions.

To obtain an analytic expression for $\epsilon(\mathbf{k})$ we have expanded $\epsilon(\mathbf{k})$ in a series of functions, each of which has the symmetry of the point group of the lattice, and performed a least-squares fit of this series to the numerical results of Burdick. This series may be written in the form

$$L(c_j,\mathbf{k})=\sum_{j=1}^{n} c_j\varphi_j(\mathbf{k}), \tag{34}$$

where the c_j are the coefficients to be determined and n is the number of functions, denoted by $\varphi_j(\mathbf{k})$, used in the approximation. For convenience we shall remove the factor $k_0=\pi/4a$ from $\mathbf{k}$, writing $\mathbf{k}=k_0\mathbf{x}$, where $\mathbf{x}=(x,y,z)$. Factoring $E_0=\hbar^2k_0^2/2m$ from the c_j and incorporating higher powers of k_0 into the c_j we write

$$L(a_j,\mathbf{x})=E_0\sum_{j=1}^{\infty} a_j\varphi_j(\mathbf{x}). \tag{35}$$

The functions $\varphi_j(\mathbf{x})$ are given in Table I.

[17] M. I. Chodorow, Ph.D. thesis, M.I.T., 1939 (unpublished).
[18] D. J. Roaf, Phil. Trans. Roy. Soc. (London) **A255**, 135 (1962).
[19] D. Shoenberg, Phil. Trans. Roy. Soc. (London) **A255**, 85 (1962).

The root-mean-square error can be written

$$L_2(\epsilon-L)=\{M^{-1}\sum_{i=1}^{M}[\epsilon(\mathbf{x}_i)-L(a_j,\mathbf{x}_i)]^2\}^{1/2}, \tag{36}$$

where $\epsilon(\mathbf{x}_i)$ is the calculated energy eigenvalue of the conduction band at $\mathbf{k}_i=k_0\mathbf{x}_i$ taken relative to $\epsilon(\Gamma_{12})$, and M is the number of values of $\mathbf{x}_i$, 2048 in this case. Taking $(\partial L_2/\partial a_j)=0$ for $j=1, 2, \cdots n$ to minimize L_2, we obtain

$$E_0\sum_{l=1}^{n} a_l[\sum_{i=1}^{M}\varphi_l(\mathbf{x}_i)\varphi_j(\mathbf{x}_i)]=\sum_{i=1}^{M}\epsilon(\mathbf{x}_i)\varphi_j(\mathbf{x}_i). \tag{37}$$

This set of equations may then be solved for the set of coefficients a_j which give the approximation having minimal root-mean-square error. These coefficients for various values of n are tabulated with the corresponding root-mean-square error in Table I.[20]

The last column in Table I shows the coefficients and root-mean-square error corresponding to the trial Fermi surface used by Pippard[21] to describe his experimental results in measurements of the anomalous skin effect in copper. This surface was of the form

$$1=x^2+y^2+z^2+A(x^2y^2+y^2z^2+z^2x^2)+Bx^2y^2z^2,$$

where $A=0.3$ and $B=-5.6$. It should be noted that this is an expression to describe the Fermi surface and was not an attempt to represent the band structure of copper.

In order to apply these results to the [111] direction it is necessary to rotate Eq. (34) so that the k_z axis lies in the $\langle 111\rangle$ direction. We use the expression for the action of the rotation operator P_R on the function $f(\mathbf{x})$, i.e., $P_Rf(\mathbf{x})=f(\mathbf{R}^{-1}\mathbf{x})$, where $\mathbf{R}$ is the rotation matrix

$$6^{-1/2}\begin{bmatrix}-\sqrt{3} & \sqrt{3} & 0\\ -1 & -1 & 2\\ \sqrt{2} & \sqrt{2} & \sqrt{2}\end{bmatrix}.$$

Equation (35) becomes

$$L_R(a_j',\mathbf{x})=E_0\sum_{j=1}^{n} a_j\varphi_j(\mathbf{R}^{-1}\mathbf{x})=E_0\sum_{j=1}^{n'} a_j'\varphi_j'(\mathbf{x}). \tag{38}$$

Using the coefficients a_j for the case $n=6$, the coefficients a_j' were calculated and are shown with the rotated functions $\varphi_j'(\mathbf{x})$ in Table II.

IV. RESULTS

In principle, if the energy is known as a function of $\mathbf{k}$, the Lorentz force equation for the motion of a Bloch

[20] The expansion for $n=10$ was used in all calculations in the $\langle 100\rangle$ directions since it is more convenient and the root-mean-square error is the same as the computational error given by Burdick. In this and later calculations the lattice constant for copper was taken to be 3.603 Å.
[21] A. B. Pippard, Phil. Trans. Roy. Soc. (London) **A250**, 325 (1957).

TABLE. I. The expansion functions $\varphi_j(\mathbf{x})$ are listed in the upper portion of the table. The coefficients a_j for $n=15$, 10, 6, and 4 are listed in the second through fifth columns of the lower portion of the table; the last column shows the results for Pippard's trial surface. The root-mean-square error in rydbergs is shown in the last row.

j	$\varphi_j(\mathbf{x})$	j	$\varphi_j(\mathbf{x})$
1	$x^2+y^2+z^2$	9	$x^2y^2z^2(x^2+y^2+z^2)$
2	$x^4+y^4+z^4$	10	$x^2y^6+y^2x^6+\cdots$
3	$x^2y^2+y^2z^2+z^2x^2$	11	$x^{10}+y^{10}+z^{10}$
4	$x^6+y^6+z^6$	12	$x^2y^8+y^2x^8+\cdots$
5	$x^2y^2z^2$	13	$x^6y^4+y^4x^6+\cdots$
6	$x^2y^4+y^2x^4+\cdots$	14	$x^2y^2z^2(x^4+y^4+z^4)$
7	$x^8+y^8+z^8$	15	$x^2y^2z^2(x^2y^2+y^2z^2+z^2x^2)$
8	$x^4y^4+y^4z^4+z^4x^4$		

j	$n=15$	$n=10$	$n=6$	$n=4$	Pippard
1	−0.2113	−0.2693	−0.2600	0.08597	0.328
2	0.006028	0.01858	0.02171	0.006731	
3	0.1068	0.07647	0.05814	0.02289	0.00218
4	0.0005733	−0.00002989	−0.0001486		
5	−0.03495	−0.01090	−0.004340	−0.002362	−0.000892
6	−0.002392	−0.0009108	−0.0005319		
7	−0.00001142	−0.000001508			
8	0.00007959	−0.00001131			
9	0.001113	0.0001023			
10	0.00001453	0.000007448			
11	0.00000005218				
12	0.0000001076				
13	−0.0000007571				
14	−0.000008421				
15	−0.00002446				
L_2	0.0095	0.0111	0.0212	0.0298	0.106

electron

$$c\hbar(d\mathbf{k}/du)=-e(\mathbf{v}\times\mathbf{B}) \tag{39}$$

can be solved for $\mathbf{k}(u)$ using $\hbar\mathbf{v}=\nabla_k\epsilon$. This solution can be substituted in the expression for $\mathbf{v}(\mathbf{k})$ to obtain $\mathbf{v}(u)$ from which the coefficients $\bar{v}$, v_l, and $w_l^{\pm}$ of Eqs. (24) and (25) can be found. However, except for special cases, e.g., when the Fermi surface exhibits cylindrical symmetry about the magnetic field, Eq. (39) is quite difficult to solve exactly.

Setting $L(c_j,\mathbf{k})$ from Eq. (34) equal to $\epsilon(\mathbf{k})$ in Eq. (21) we may approximate the expansion of Eq. (21). This expansion may be set equal to ϵ_F, the Fermi energy, and $k_\perp$, the transverse component of the electron wave vector on the Fermi surface, can be found by doing a perturbation calculation for ρ. The zeroth-order approximation gives the equation

$$\epsilon_F=\epsilon_0(\rho_0,k_z), \tag{40}$$

which may be solved for $\rho_0(k_z)$. The first-order correction is

$$\rho_1=-\frac{2\epsilon_1(\rho_0,k_z)}{(\partial\epsilon_0/\partial\rho)(\rho_0,k_z)}\cos p\varphi\equiv k_1\cos p\varphi, \tag{41}$$

where $k_0=\rho_0$ and k_1 are the $l=0$ and 1 terms of the expansion

$$k_\perp=\sum_{l=0}^{\infty}k_l\cos pl\varphi. \tag{42}$$

The quantities $k_0(k_z)$ and $k_1(k_z)$ are shown in Figs. 1 and 2 for the ⟨100⟩ and ⟨111⟩ directions, respectively. In Fig. 2, inexactness of the fit of $L(c_j,\mathbf{k})$ to the energy eigenvalues caused the computed value of k_0 near the neck to fall below the observed value.[22] The dotted curve shows the correction made to bring k_0 into agreement with the observed neck radius.

We substitute Eq. (42) in the expression $\hbar v_z=\partial\epsilon(\rho,\varphi,k_z)/\partial k_z$ for ρ to obtain a series in $\cos pl\varphi$, the coefficients of which are $\bar{v}$ and v_l of Eq. (25). Figures 3 and 4 show $\bar{v}(k_z)$, $v_1(k_z)$, and $v_2(k_z)$ evaluated on the Fermi surface for the ⟨100⟩ and ⟨111⟩ directions, respectively. In Fig. 4, v_2 is essentially zero for all values of k_z. Also, $\bar{v}$ is terminated at the k_z value for which k_0 became smaller than the neck radius (see Fig. 2). Intuitively, $\bar{v}$ should go to zero as k_z approaches its maximum value

TABLE II. The expansion functions $\varphi_j'(\mathbf{x})$ and the coefficients a_j' are listed. The first column shows the value of j, the second a_j', and the third $\varphi_j'(\mathbf{x})$.

j	a_j'	φ_j'
1	−0.2600	$x^2+y^2+z^2$
2	0.02538	$(x^2+y^2)^2$
3	−0.006939	$yz(y^2-3x^2)$
4	0.04342	$z^2(x^2+y^2)$
5	0.02662	z^4
6	−0.0001701	$(x^2+y^2)^3$
7	−0.00005907	$y^2(y^2-3x^2)^2$
8	0.0002913	$yz(x^2+y^2)(y^2-3x^2)$
9	−0.0007332	$z^2(x^2+y^2)^2$
10	−0.0001266	$z^3y(y^2-3x^2)$
11	−0.0001200	$z^4(x^2+y^2)$
12	−0.0002954	z^6

[22] H. V. Bohm and V. J. Easterling, Phys. Rev. **128**, 1021 (1962).

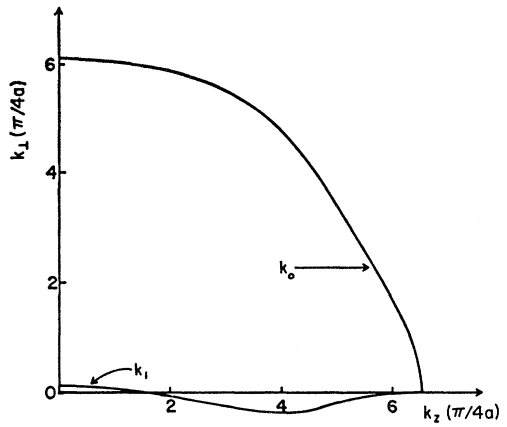

FIG. 1. $k_0(k_z)$ and $k_1(k_z)$ for the [100] direction.

in the ⟨111⟩ direction. However, this need not be true because the Brillouin zone of the fcc lattice does not contain a reflection plane perpendicular to the ⟨111⟩ direction.

The coefficients $w_l^{\pm}$ of $v^{\pm}$ may be found in a similar manner. However, these coefficients are obtained much more simply by writing Eq. (39) in circularly polarized notation,

$$\frac{dk_{\pm}}{du}=\pm i\frac{eB}{\hbar c}v_{\pm}. \tag{43}$$

Using $k_{\pm}=k_1 e^{\pm i\varphi}$ and Eqs. (24) and (42), we obtain upon equating coefficients

$$w_l^{\pm}=\pm\frac{\hbar}{m_c}\left[\frac{k_l}{2}(pl\pm 1)\pm\frac{k_0}{2}\delta(l,0)\right]. \tag{44}$$

The coefficients $w_0(k_z)$, $w_1^{+}(k_z)$, and $w_1^{-}(k_z)$ are shown in Figs. 5 and 6 for the ⟨100⟩ and ⟨111⟩ directions.

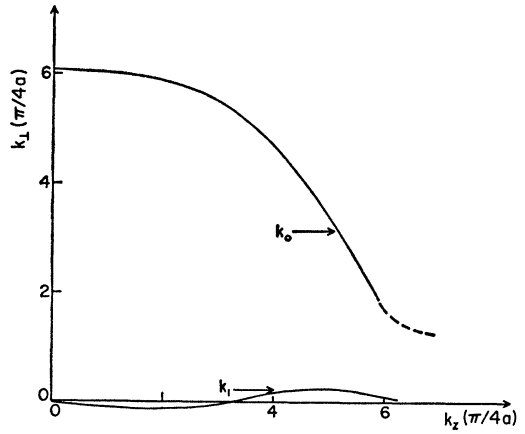

FIG. 2. $k_0(k_z)$ and $k_1(k_z)$ for the ⟨111⟩ direction.

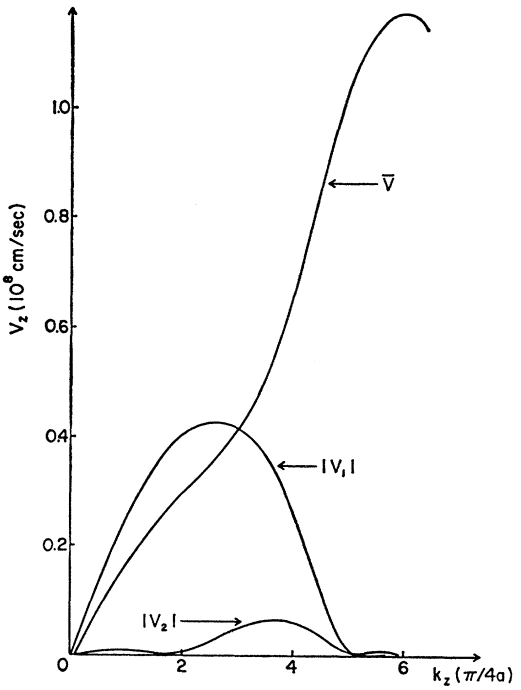

FIG. 3. $\bar{v}(\epsilon_F,k_z)$ and the absolute values of $v_1(\epsilon_F,k_z)$ and $v_2(\epsilon_F,k_z)$ for the ⟨100⟩ direction.

Figure 6 was terminated in the same manner as Fig. 4.

The cyclotron effective mass m_c of an electron, defined in Eq. (18), can be found from a result given by

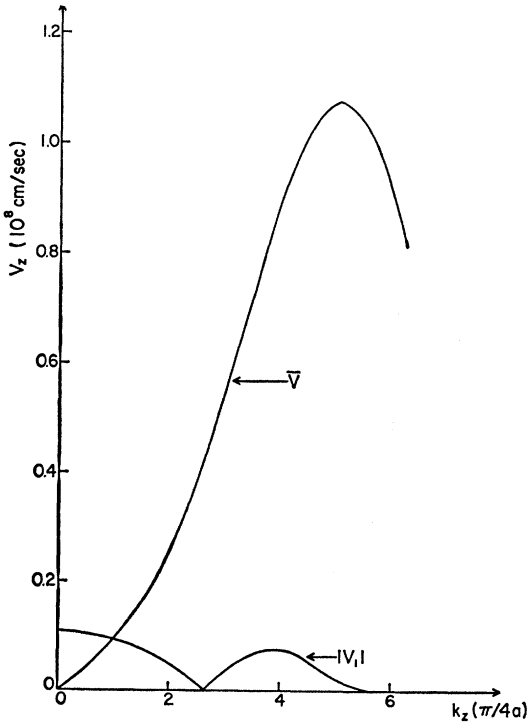

FIG. 4. $\bar{v}(\epsilon_F,k_z)$ and the absolute value of $v_1(\epsilon_F,k_z)$ for the ⟨111⟩ direction.

Harrison[23]:

$$2\pi m_c\bar{v}=-h(\partial S/\partial k_z), \tag{45}$$

where $S(k_z)$ is the cross-sectional area of the Fermi surface at k_z. Using Eq. (42) we find

$$S(k_z)=\int_0^{2\pi}\int_0^{k_1} k_1 dk_1 d\varphi=\pi(k_0^2+\tfrac{1}{2}\sum_{l=1}^{\infty} k_l^2). \tag{46}$$

This expression was differentiated numerically to obtain $m_c(k_z)$ shown in Fig. 7 for the ⟨100⟩ and ⟨111⟩ directions. These curves agree with the experimental[24] values for the cyclotron effective mass of 1.385 at $k_z=0$ in the ⟨100⟩ direction, 1.355 at $k_z=0$, and 0.6 on the neck

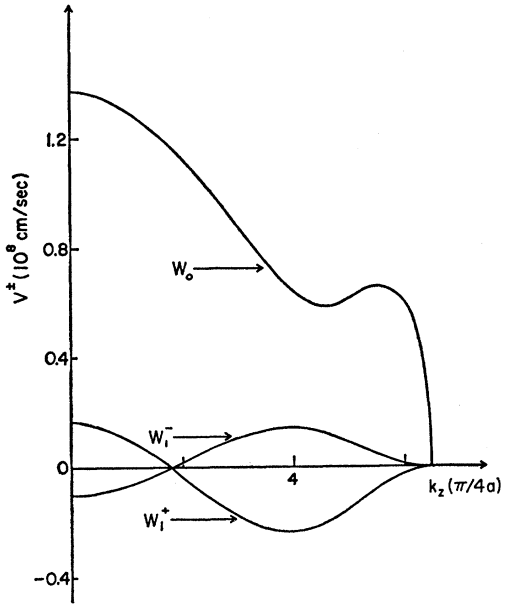

FIG. 5. $w_0(\epsilon_F,k_z)$, $w_1^{\pm}(\epsilon_F,k_z)$ for ⟨100⟩ direction.

in the ⟨111⟩ direction. The dotted portion of the curve for the ⟨111⟩ direction was obtained by linear extrapolation.

Assuming that $w_l^{\pm}$ and v_l are negligible for $l\geq 2$, Eq. (33) reduces to

$$\sigma_{\pm}=\frac{e^3B_0}{(2\pi)^3\hbar^2c}\sum_{l=-\infty}^{\infty}\int dk_z\, T(\epsilon_F,k_z)$$
$$\times[w_0J_l(X_1)+w_1^{\pm}J_{l-1}(X_1)+w_1^{\mp}J_{l+1}(X_1)]^2$$
$$\times\left\{\frac{1}{\tau}+i[\omega-(pl\pm 1)\omega_c-q\bar{v}]\right\}^{-1}. \tag{47}$$

[23] W. A. Harrison, Phys. Rev. **118**, 1190 (1960).
[24] A. F. Kip, D. N. Langenberg, and T. W. Moore, Phys. Rev. **124**, 359 (1961).

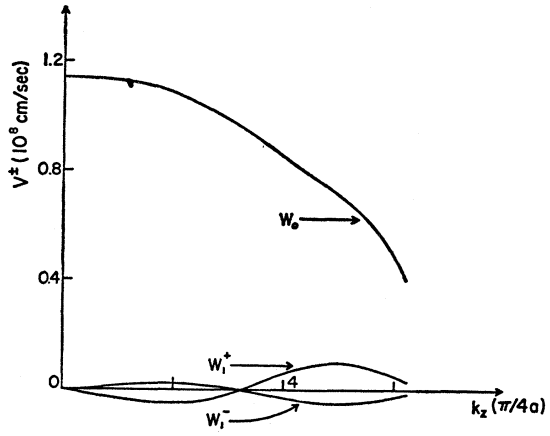

FIG. 6. $w_0(\epsilon_F,k_z)$, $w_1^{\pm}(\epsilon_F,k_z)$ for ⟨111⟩ direction.

Using the results shown in Figs. 1–7 this integration can be performed numerically. Equation (15) can now be solved for the dispersion formula $\omega(q,B_0)$. The experimental conditions are such that ω is kept fixed, so that we should solve Eq. (15) for $q=q_1-iq_2$ for fixed ω. However, it is more convenient, and equally correct because the velocity of sound changes very little from its value in the absence of electron interactions and because $q_2\ll q_1$, to solve for $\omega=\omega_1+i\omega_2$ for fixed q given by $\omega_0=sq$, ω_0 being the frequency of the externally applied sound field.[3] The coefficient of attenuation γ is given by

$$\gamma=2\omega_2/s. \tag{48}$$

The difference in velocities of the right- and left-circularly polarized components of a linearly polarized

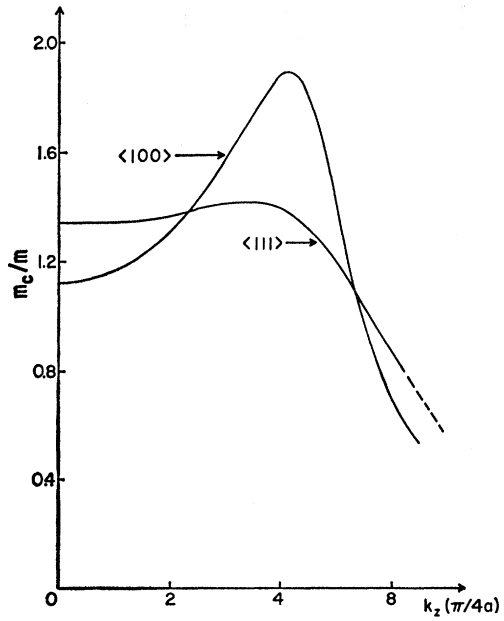

FIG. 7. $m_c(k_z)/m$ for ⟨100⟩ and ⟨111⟩ directions.

shear wave gives rise to a rotation of the plane of polarization of the sound wave given by

$$\Delta\theta/L=\Delta\omega_1/2s, \tag{49}$$

where $\Delta\omega_1$ is the difference in the real parts of the frequencies of the two circular polarizations and L is the length of the sample.

The velocity of transverse sound in the ⟨100⟩ direction, determined from measurements of the low-temperature elastic constants by Overton and Gaffney,[25] was taken to be 3.011×10^5 cm/sec. The coefficient of attenuation γ is shown in Figs. 8 and 9 for frequencies of 110, 50, and 30 Mc/sec where we have taken the electron collision time τ to be such that $\omega_c\tau$ at 18 kG is 50 and 10, respectively. The rotation of the plane of polarization for the above frequencies and the larger collision time is shown in Fig. 10.

The velocity of transverse sound in the ⟨111⟩ direction, found in the same manner as above,[25] was taken to be 2.217×10^5 cm/sec. The coefficient of attenuation and the rotation of the plane of polarization of a shear acoustic wave propagating in the ⟨111⟩ direction are shown in Figs. 11, 12, and 13 for the same conditions described above for Figs. 8, 9, and 10.

Figure 14 shows the product $(m_c\bar{v}/m)$ versus k_z for the ⟨100⟩ and ⟨111⟩ directions. Using Eq. (3) we find that the Kjeldaas edge should occur at 20.2 and 24 kG for the ⟨100⟩ and ⟨111⟩ directions, respectively. The edge occurs at a larger field in the ⟨111⟩ direction because the velocity of transverse sound is considerably smaller than in the ⟨100⟩ direction. The large peak in the coefficient of attenuation at magnetic fields just below

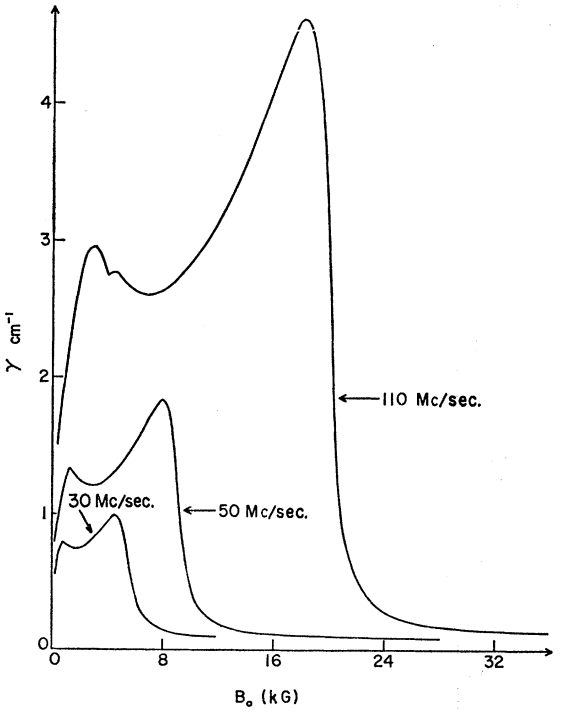

FIG. 8. The attenuation coefficient γ of a shear wave propagating in the ⟨100⟩ direction for frequencies of 110, 50, and 30 Mc/sec and $\omega_c(18)\tau=50$. This corresponds to a ql that is 57 at 110 Mc/sec and scaled appropriately at lower frequencies.

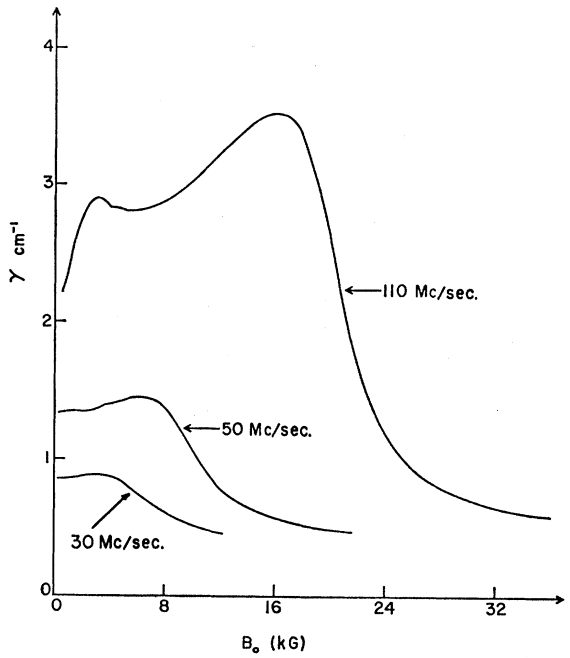

FIG. 9. The attenuation coefficient γ of a shear wave propagating in the ⟨100⟩ direction for frequencies of 110, 50, and 30 Mc/sec and $\omega_c(18)\tau=10$. This corresponds to a ql that is 11.4 at 110 Mc/sec and scaled appropriately at lower frequencies.

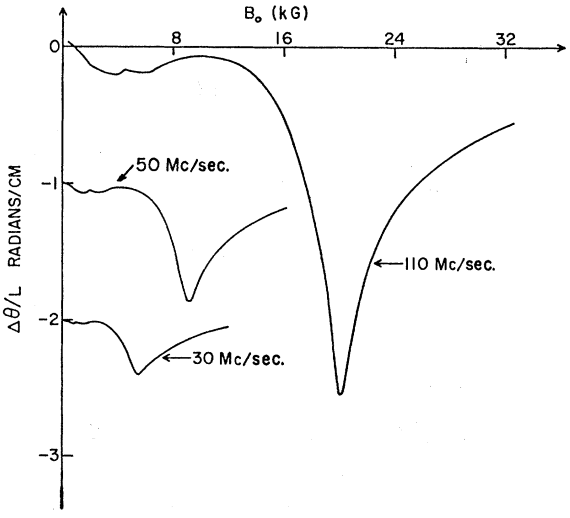

FIG. 10. The rotation of the plane of polarization of a shear wave propagating in the ⟨100⟩ direction for the conditions of Fig. 8. The origins of the 50 Mc/sec curve and the 30 Mc/sec curve have been shifted downward 1 and 2 rad/cm, respectively.

[25] W. C. Overton, Jr. and J. Gaffney, Phys. Rev. 98, 969 (1955).

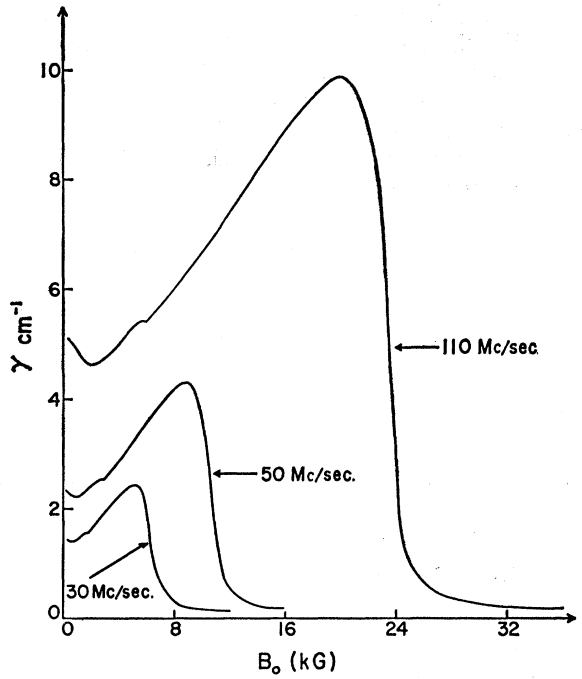

FIG. 11. The attenuation coefficient γ of a shear wave propagating in the ⟨111⟩ direction for frequencies of 100, 50, and 30 Mc/sec and $\omega_c(18)\tau=50$. This corresponds to a ql that is 78 at 110 Mc/sec and scaled appropriately at lower frequencies.

the Kjeldaas edge results from the fact that two groups of electrons with different values of positive k_z satisfy Eq. (3). The small dips in the coefficient of attenuation and the rotation of the plane of polarization in the ⟨100⟩

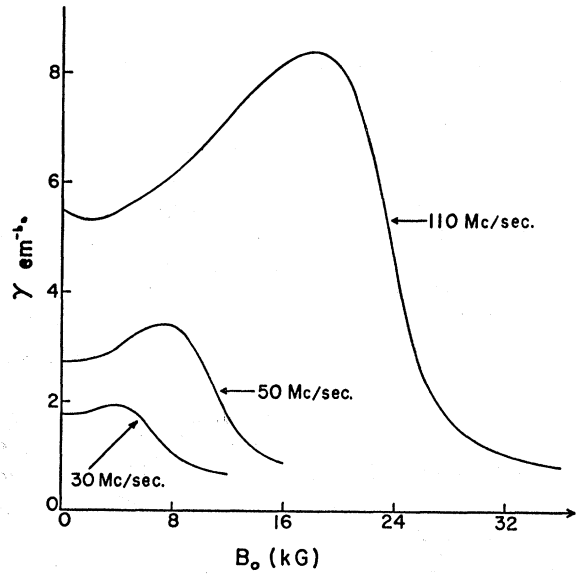

FIG. 12. The attenuation coefficient γ of a shear wave propagating in the ⟨111⟩ direction for frequencies of 110, 50, and 30 Mc/sec and $\omega_c(18)\tau=10$. This corresponds to a ql that is 15.5 at 110 Mc/sec and scaled appropriately at lower frequencies.

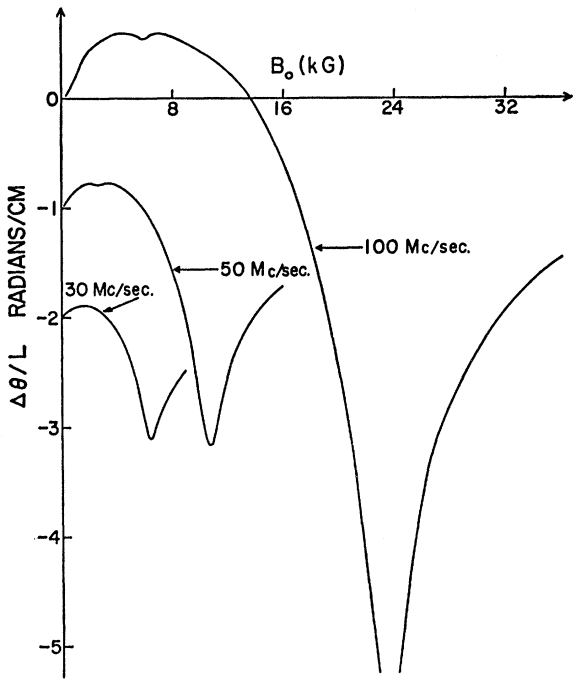

FIG. 13. The rotation of the plane of polarization of a shear wave propagating in the ⟨111⟩ direction for the conditions of Fig. 11. The origins of the 50 Mc/sec curve and the 30 Mc/sec curve have been shifted downward 1 and 2 rad/cm, respectively.

direction at $B_0=4.0$ kG as seen in the 110 Mc/sec curves of Figs. 8 and 10 result from a resonance[7] in the magnetoconductivity tensor σ [see Eq. (47)] at the magnetic field for which

$$q\bar{v}=5\omega_c. \tag{50}$$

Similar resonances should occur at the magnetic field

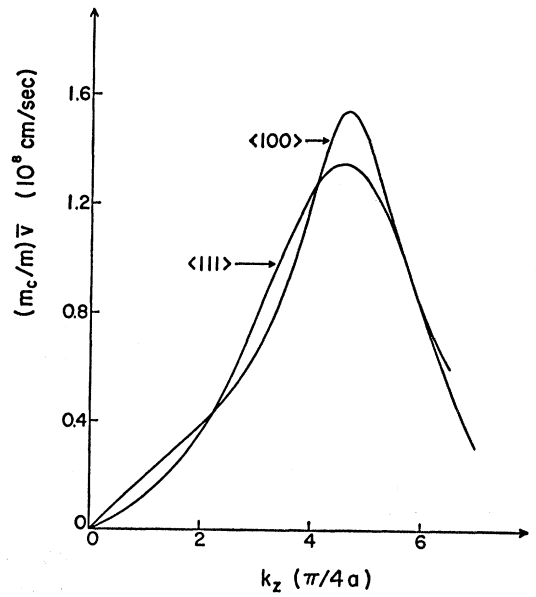

FIG. 14. $(m_c\bar{v}/m)$ versus k_z for the ⟨100⟩ and ⟨111⟩ directions.

(6.8 kG) for which

$$q\bar{v}=3\omega_c. \tag{51}$$

The magnitude of these resonances depends upon the magnitude of $w_1^{\pm}$ and since w_1^{+} corresponding to Eq. (50) is larger than w_1^{-} corresponding to Eq. (51) for all values of k_z, the resonance at $B_0=6.8$ kG is obscured. (By making $w_1^{\pm}$ unrealistically large, resonances at $B_0=6.8$ kG appear.) These resonances disappear at lower frequencies and lower collision times. In the ⟨111⟩ directions $w_1^{\pm}$ is very small for all k_z and, hence, these resonances are essentially unobservable in all the curves of Figs. 11–13.

The peak in the coefficient of attenuation in the ⟨100⟩ directions which occurs at 3.0 kG for a frequency of 110 Mc/sec and at corresponding lower fields for lower frequencies (see Figs. 8 and 9) may be identified with the peak observed by Boyd and Gavenda[7] and discussed by other authors.[7,26] This peak is associated with the presence of the Bessel functions in the conductivity tensor and, hence, should be described in quantum-mechanical language as a geometrical resonance. That is, it results from a variation in the matrix elements rather than a variation in the resonant denominator.

[26] S. G. Eckstein, Phys. Rev. Letters **16**, 611 (1966).

PHYSICAL REVIEW VOLUME 157, NUMBER 3 15 MAY 1967

Nuclear Quadrupole Coupling, Knight Shift, and Spin-Lattice Relaxation Time in Beryllium Metal*

D. E. Barnaal,† R. G. Barnes, B. R. McCart,‡
L. W. Mohn,§ and D. R. Torgeson
Institute for Atomic Research and Department of Physics, Iowa State University, Ames, Iowa

(Received 23 December 1966)

The nuclear quadrupole coupling and Knight shift of Be^9 have been measured in high-purity beryllium metal at room temperature and at 77°K in magnetic-field strengths up to 25 kOe. The nuclear quadrupole coupling constant is found to have the value $e^2qQ/h=61.8\pm1.8$ kHz, independent of temperature. By contrast, the best estimate of the lattice contribution to the quadrupole coupling is found to be 68 ± 6 kHz, which implies that the conduction-electron contribution opposes that of the lattice. The Knight shift is found to have the values $K_{Be}=-0.0025\pm(6)$ at 300°K and $K_{Be}=-0.0035\pm(6)$ at 77°K (in percent); the uncertainty given is the standard deviation of the measurements. Measurements of the spin-lattice relaxation time at two temperatures indicate that $T_1T=1.66\times10^4$ sec °K with an uncertainty of 10%. These experimental observations can be interpreted in terms of direct-contact and core-polarization contributions, from a predominantly p-like band, which partially cancel to yield the small Knight shift.

INTRODUCTION

THE nuclear quadrupole coupling in beryllium metal has been of interest both from the solid-state and nuclear standpoints. From the theoretical standpoint, the calculation of the coupling constant in beryllium by Pomerantz and Das[1] was the first to include, in an explicit manner, the contribution of the conduction electrons to the electric field gradient (EFG). That calculation, combined with the measured value of the coupling constant reported by Knight,[2] yielded a value for the quadrupole moment of Be^9 which was for some time the only available value for this quantity. Quite recently, atomic beam measurements[3] have yielded an independent value for $Q(Be^9)$ which differs significantly from that derived by Pomerantz and Das.

We report here on new measurements of the quadrupole coupling in beryllium, in which we have obtained a value 25% greater than that reported by Knight.[2] Nonetheless, this measured coupling is still less than that calculated on the basis of the atomic beam value of Be^9 and the lattice contribution to the EFG. Whereas the calculation of Pomerantz and Das indicated that the conduction-electron contribution to the EFG was of the same sign as the lattice contribution, the present results suggest that the two contributions are very likely of opposite sign. This is interesting in view of the fact that in essentially all other metallic cases the relative sign of the lattice and conduction-electron contribution is unknown.

Similarly, the unusually small Knight shift, which

* Work performed in the Ames Laboratory of the U. S. Atomic Energy Commission. Contribution No. 2010.

† Summer Faculty Participant. Permanent address: Luther College, Decorah, Iowa.

‡ Summer Faculty Participant. Permanent address: Augustana College, Rock Island, Illinois.

§ Present address: University of Washington, Seattle, Washington.

[1] M. Pomerantz and T. P. Das, Phys. Rev. **119**, 70 (1960).

[2] W. D. Knight, Phys. Rev. **92**, 539 (1953).

[3] A. G. Blachman and A. Lurio, Bull. Am. Phys. Soc. **11**, 343 (1966).